

# Density-Matrix Propagation Driven by Semiclassical Correlation

Peter Elliott<sup>[a]</sup> and Neepa T. Maitra<sup>\*[b,c]</sup>

Methods based on propagation of the one-body reduced density-matrix hold much promise for the simulation of correlated many-electron dynamics far from equilibrium, but difficulties with finding good approximations for the interaction term in its equation of motion have so far impeded their application. These difficulties include the violation of fundamental physical principles such as energy conservation, positivity conditions on the density, or unchanging natural orbital occupation numbers. We review some of the recent efforts to confront these problems, and explore a semiclassical approximation for electron correlation coupled to time-dependent

Hartree-Fock propagation. We find that this approach captures changing occupation numbers, and excitations to doubly-excited states, improving over TDHF and adiabatic approximations in density-matrix propagation. However, it does not guarantee  $N$ -representability of the density-matrix, consequently resulting sometimes in violation of positivity conditions, even though a purely semiclassical treatment preserves these conditions. © 2016 Wiley Periodicals, Inc.

DOI: 10.1002/qua.25087

## Introduction

Time-resolved dynamics of electrons in atoms, molecules, and solids are increasingly relevant for a large class of problems today. The electrons and ions are excited far from their ground states in photo-induced processes such as in photovoltaics or laser-driven dynamics, and control of the dynamics on the attosecond time-scale is now experimentally possible. To theoretically model these processes an adequate accounting of electron correlation is required. Clearly solving the full time-dependent Schrödinger equation (TDSE) is impossible for more than a few electrons, and, moreover, the many-electron wavefunction contains much more information than is needed. Most observables of interest involve one- or two-body operators, suggesting that a description in terms of reduced variables would be opportune: in particular, obtaining directly just the one- and two-body time-dependent reduced density matrices (TD RDMs)<sup>[1]</sup> would enable us to obtain any one- or two-body observable (e.g., electron densities, momentum profiles, double-ionization probabilities, etc). Even simpler, the theorems underlying time-dependent density functional theory (TDDFT) prove that *any* observable can be obtained from knowledge of simply the one-body density. However, hiding in any of these reduced descriptions is the complexity of the full many-body interacting electron problem, in the form of reconstruction functionals for the RDM case and exchange-correlation potentials as well as observable-functionals in the TDDFT case. In practice, these terms must be approximated, and intense research has been underway in recent years to determine approximations that are accurate but practically efficient. The temptation to simply use approximations that were developed for the ground-state cases, whose properties for the ground-state have been well-studied and understood, has proved profitable in some cases giving, for example, usefully

accurate predictions of excitation spectra.<sup>[2–4]</sup> But when used for non-perturbative dynamics, these same approximations can become rapidly unreliable. These problems will be reviewed in the next section.

Solving the full TDSE scales exponentially with the number of electrons in the system, while the computational cost of propagating RDMs is in principle independent of the system-size. Classical dynamics of many-body systems on the other hand scales linearly with the number of particles, which raises the question of using semiclassical approaches to many-electron systems. Usually used for nuclear dynamics, a semiclassical wavefunction is built using classical dynamical information alone, in particular the phase arises from the classical action along the trajectory<sup>[5–10]</sup>; in this way semiclassical methods can capture essential quantum phenomena such as interference, zero-point energy effects, and to some extent tunneling.

We present some results from an approach that uses semiclassical electron dynamics to evaluate the correlation term in the propagation of the reduced density-matrix, with all the other terms in the equation of motion treated exactly, as introduced in Refs. [11,12]; thus it is a semiclassical-correlation driven time-dependent Hartree-Fock (TDHF). We study dynamics in perturbative and non-perturbative fields in two one-dimensional (1D) model systems of two electrons: one is a Hooke's atom, and the other a soft-Coulomb Helium atom.

[a] P. Elliott  
Max-Planck-Institut Für Mikrostrukturphysik, Halle D-06120, Germany

[b] N. T. Maitra  
Department of Physics and Astronomy, Hunter College and the City  
University of New York, New York, New York 10016. E-mail: nmaitra@  
hunter.cuny.edu

[c] N. T. Maitra  
Physics Program, the Graduate Center, CUNY, New York, New York 10016

© 2016 Wiley Periodicals, Inc.

The method improves over both TDHF and the pure semiclassical method for the dynamics and excitation spectra in the Hooke's atom case, but gives unphysical negative density regions in the soft-Coulomb case. This is due to violation of  $N$ -representability conditions, even though the pure semiclassical dynamics and the TDHF on their own preserve these conditions.

### Propagating reduced density matrices: A brief review

We start with the TDSE for the electron dynamics of a given system (defined by the external potential,  $v_{\text{ext}}(\mathbf{r})$ ):

$$i\dot{\Psi}(x_1 \dots x_N, t) = \left( \sum_j -\nabla_j^2/2 + \sum_j v_{\text{ext}}(\mathbf{r}_j) + \sum_{i<j} v_{\text{INT}}(\mathbf{r}_i, \mathbf{r}_j) \right) \Psi(x_1 \dots x_N, t) \quad (1)$$

where  $x = (\mathbf{r}, \sigma)$  is a combined spatial and spin index,  $\Psi$  is the wavefunction, and  $v_{\text{INT}}$  is the 2-body Coulomb interaction between the electrons,  $v_{\text{INT}}(\mathbf{r}, \mathbf{r}') = 1/|\mathbf{r} - \mathbf{r}'|$ . Atomic units are used throughout this paper, ( $m_e = \hbar = e^2 = 1$ ). Additionally, the initial wavefunction  $\Psi_0$  must be specified in order to begin the propagation. However solving Eq. (1) is computationally an extremely costly exercise and becomes intractable as the number of electrons in the system grows. Thus we must seek an alternative approach that aims to reproduce the result of Eq. (1) but at a much more reasonable computational cost. Further, as mentioned in the introduction, the many-electron wavefunction contains far more information than one usually needs.

Most observables that are experimentally measurable or of interest involve one- and two-body operators, such as the density e.g. in dipole/quadrupole moments, the momentum-density e.g. in Compton profiles, and pair-correlation functions in e.g. double-ionization. So a formulation directly in terms of one- and two-body density-matrices, bypassing the need to compute the many-electron wavefunction, would be more useful.

This leads to the concept of reduced density-matrices, where the  $p$ -RDM involves tracing the full  $N$ -electron wavefunction over  $N - p$  degrees of freedom:

$$\rho_p(x'_1 \dots x'_p, x_1 \dots x_p, t) = \frac{N!}{(N-p)!} \int dx_{p+1} \dots dx_N \Psi^*(x'_1 \dots x'_p, x_{p+1} \dots x_N, t) \Psi(x_1 \dots x_p, x_{p+1} \dots x_N, t) \quad (2)$$

The diagonal of the  $p$ -RDM gives the  $p$ -body density,  $\Gamma(x_1 \dots x_p, t)$ , the probability of finding any  $p$  electrons at points  $\mathbf{r}_1 \dots \mathbf{r}_p$  with spin  $\sigma_1 \dots \sigma_p$  at time  $t$ . One can also define spin-summed RDMs: e.g.  $\rho_1(\mathbf{r}', \mathbf{r}, t) = \sum_{\sigma, \sigma_2, \dots, \sigma_N} \rho_1(x', x, t)$ . The Bogoliubov–Born–Green–Kirkwood–Yvon (BBGKY) hierarchy of equations of motion for the RDMs were written down sixty years ago<sup>[13,14]</sup>. The first in the hierarchy is that for  $\rho_1$ , which spin-summed is:

$$i\dot{\rho}_1(\mathbf{r}', \mathbf{r}, t) = \left( -\nabla^2/2 + v_{\text{ext}}(\mathbf{r}, t) + \nabla'^2/2 - v_{\text{ext}}(\mathbf{r}', t) \right) \rho_1(\mathbf{r}', \mathbf{r}, t) + \int d^3r_2 f_{ee}(\mathbf{r}, \mathbf{r}', \mathbf{r}_2) \rho_2(\mathbf{r}', \mathbf{r}_2, \mathbf{r}, \mathbf{r}_2, t) \quad (3)$$

where

$$f_{ee}(\mathbf{r}, \mathbf{r}', \mathbf{r}_2) = v_{\text{INT}}(\mathbf{r}, \mathbf{r}_2) - v_{\text{INT}}(\mathbf{r}', \mathbf{r}_2) \quad (4)$$

The electron-interaction term in the equation for the 1RDM involves the 2RDM, whose equation of motion, the second in the hierarchy,

$$i\dot{\rho}_2(\mathbf{r}'_1, \mathbf{r}'_2, \mathbf{r}_1, \mathbf{r}_2, t) = \left( \sum_{i=1,2} \left( (-\nabla_i^2/2 + v_{\text{ext}}(\mathbf{r}_i, t)) - \left( -\nabla_i'^2/2 + v_{\text{ext}}(\mathbf{r}'_i, t) \right) + v_{\text{INT}}(\mathbf{r}_1, \mathbf{r}_2) - v_{\text{INT}}(\mathbf{r}'_1, \mathbf{r}'_2) \right) \rho_2(\mathbf{r}'_1, \mathbf{r}'_2, \mathbf{r}_1, \mathbf{r}_2, t) + \int d^3r_3 (f_{ee}(\mathbf{r}_1, \mathbf{r}'_1, \mathbf{r}_3) + f_{ee}(\mathbf{r}_2, \mathbf{r}'_2, \mathbf{r}_3)) \rho_3(\mathbf{r}_1, \mathbf{r}_2, \mathbf{r}_3, \mathbf{r}'_1, \mathbf{r}'_2, \mathbf{r}_3, t) \right) \quad (5)$$

involves the 3RDM, and so on. Solving the full hierarchy is equivalent to solving Eq. (1) and no less impractical for many-electron systems. The hierarchy is usually therefore truncated, typically using a "cluster expansion" where one reconstructs higher-order RDMs as antisymmetrized products of lower order ones plus a correlation term, sometimes referred to as a cumulant. Putting the correlation term to zero becomes exact for the case when the underlying wavefunction is a single Slater determinant (SSD). For example, in the case of truncation at the first equation, the equations reduce to TDHF, and, for a spin singlet of a closed shell system,  $\rho_2$  in Eq. (3) is replaced by,

$$\rho_2^{\text{SSD}}(\mathbf{r}', \mathbf{r}_2, \mathbf{r}, \mathbf{r}_2, t) = \rho(\mathbf{r}_2, t) \rho_1(\mathbf{r}', \mathbf{r}, t) - \frac{1}{2} \rho_1(\mathbf{r}', \mathbf{r}_2, t) \rho_1(\mathbf{r}_2, \mathbf{r}, t) \quad (6)$$

If instead, the truncation is done at the second equation in the BBGKY hierarchy, putting the correlation term to zero in  $\rho_3$ , one obtains the Wang and Cassing approximation.<sup>[15,16]</sup> One has then the choice of propagating the equation for  $\rho_2$  alone or propagating it simultaneously alongside the equation for  $\rho_1$ .<sup>[17]</sup> However, recently it was found that, in the former case, propagating while neglecting the three-particle correlation term leads to the eventual violation of energy conservation.<sup>[17,18]</sup> Now the  $p$ -RDM can be obtained from higher-order RDMs via contraction (i.e., partial trace),

$$\rho_p(x'_1 \dots x'_p, x_1 \dots x_p, t) = \frac{1}{N-p} \int dx_{p+1} \rho_{p+1}(x'_1 \dots x'_p, x_{p+1}, x_1 \dots x_p, x_{p+1}, t) \quad (7)$$

as follows from the definition Eq. (2). So an important condition to consider when formulating reconstructions is whether they are contraction-consistent, i.e. whether they satisfy Eq. (7). In fact, in Ref. [18], it was shown that the reconstruction approximation of Refs. [15,16] violated this condition; the

underlying reason was that the spin-decomposed three-particle cumulant,<sup>[19]</sup> neglected in this approximation, has non-zero contraction. This realization enabled the authors of Ref. [18] to derive a “contraction-consistent” reconstruction for  $\rho_3$  by including the part of the three-particle cumulant that has non-zero contraction, which fortunately is exactly known as a functional of the 2RDM. This was able to conserve energy in the dynamical simulations. However, one cannot breathe easy just yet: propagation with this contraction-consistent reconstruction violated  $N$ -representability, another fundamental set of conditions that wreak havoc if not satisfied. Ref. [17] showed that contraction-consistency, and energy conservation, can be enforced if both 1RDM and 2RDM are propagated simultaneously, even while neglecting the three-particle correlation term. However again,  $N$ -representability was violated in this approach, leading to unphysical dynamics, instabilities and regions of negative densities.

$N$ -representability means that there exists an underlying many-electron wavefunction whose contraction via Eq. (2) yields the matrix in question.<sup>[20,21]</sup> For 1RDMs, the  $N$ -representability conditions are simple, and usually expressed in terms of its eigenvalues  $\eta_j$ , called natural orbital (NO) occupation numbers, as defined via:

$$\rho_1(\mathbf{r}', \mathbf{r}, t) = \sum_j \eta_j(t) \zeta_j^*(\mathbf{r}', t) \zeta_j(\mathbf{r}, t) \quad (8)$$

for the spin-summed singlet case, where  $\zeta_j(\mathbf{r}, t)$  are natural orbitals. The  $N$ -representability conditions are that  $0 \leq \eta_j \leq 2$ , and  $\sum_j \eta_j = N$ . (For the spin-resolved case, the first condition becomes  $0 \leq \eta_j \leq 1$ ). The 1RDM should be positive semi-definite, with trace equal  $N$ , and each eigenvalue bounded above by 2. If this is violated, densities can become negative in places, even when the norm is conserved. (Note that it can be shown that particle number is always conserved by any approximation<sup>[17]</sup>). For 2RDMs, only very recently has a complete set of conditions for ensemble  $N$ -representability been discovered<sup>[21]</sup>; for pure states, not all the conditions are known, although some are. One important condition regards positive semi-definiteness of the 2RDM, which is challenging to maintain in dynamics when using approximate reconstructions. Yet without positive semi-definiteness, the propagation becomes unstable. The condition is in fact violated even by the contraction-consistent reconstruction introduced in Ref. [18] and by the joint 1RDM and 2RDM propagation in Ref. [17]. Even for ground-state problems (where the analog of the BBGKY equations is referred to as the contracted Schrödinger equation), the reconstruction functionals can violate such conditions, and iterative “purification” schemes have been introduced to yield self-consistent  $N$ -representable ground-state solutions.<sup>[22,23]</sup> Even when the initial RDM satisfies  $N$ -representability conditions, one can find violations building up at later times in the propagation when approximate reconstruction functionals are used.<sup>[17,18]</sup> Ref. [18] presented promising results where a dynamical purification scheme was applied at each time-step in the dynamics of molecules in strong-fields, leading to stable and accurate propagation. A similar method<sup>[24]</sup>

uses an energy-optimization procedure to obtain the 2RDM at each time-step while also enforcing various  $N$ -representability conditions, but the resulting dynamics is unable to change occupation numbers.

From a different angle, it has been recently shown that the BBGKY equations can be recast into a Hamiltonian formulation,<sup>[25]</sup> that opens the possibility of using advanced approximate methods of classical mechanics to analyze the equations and derive different reconstructions, in terms of equivalent classical variables.

On the other hand, “time-dependent density-matrix functional theory” (TDDMFT),<sup>[26]</sup> which deals only with Eq. (3), proceeds from a somewhat different philosophy: the idea is that the 2RDM and all observables can in principle be obtained *exactly* from the time-dependent 1RDM due to the Runge–Gross theorem of TDDFT. The latter theorem<sup>[3,27]</sup> proves that given an initial state, there is a one-to-one mapping between the time-evolving one-body density ( $\rho(\mathbf{r}, t)$ , diagonal of the 1RDM), and the externally applied potential. This means that, in principle, knowledge of  $\rho(\mathbf{r}, t)$  is enough to determine the many-electron wavefunction, up to a purely time-dependent phase, and hence all pRDMs also. Since  $\rho_1(\mathbf{r}, \mathbf{r}, t) = \rho(\mathbf{r}, t)$ , this means in turn that  $\rho_1(\mathbf{r}', \mathbf{r}, t)$  determines all properties of the system. The only assumption is that time-evolution of  $\rho_1$  occurs in a local potential, meaning a multiplicative operator in space, which raises questions about  $v$ -representability.<sup>[28]</sup>

There has been significant effort to approximate the 2RDM of Eq. (3) as a functional of  $\rho_1$ , or of its NOs and occupation numbers [Eq. (8)]. A natural starting point is to insert the time-evolving 1RDM into an approximation developed for ground-state density-matrix functional theory,<sup>[29–34]</sup> thus making an “adiabatic” approximation. These functionals can give very good approximations for ground-state properties, especially important for strongly-correlated systems where common approximations in alternative scalable methods like density-functional theory fail. However, when used in time-propagation, these same functionals keep the occupation numbers fixed,<sup>[35–39]</sup> which leads to erroneous dynamics. The first real-time non-perturbative application of TDDMFT<sup>[36]</sup> resorted to an extra energy-minimizing procedure to determine occupation numbers at each time-step that resulted in time-evolving occupation numbers. By considering perturbations around the ground-state, a frequency-dependent response theory can be formalized<sup>[35]</sup> from which excitation energies can be computed, and it was shown that adiabatic functionals cannot capture double-excitations. Phase-including NO (PINO) functional theory<sup>[39–41]</sup> has been introduced to overcome this problem. Here the functional depends on the phase of the NO, which extends out of the realm of TDDMFT since any phase-dependence of the NOs cancels out when  $\rho_1$  is formed.

Computationally, it has been argued that there is an advantage to propagating the NOs and occupation numbers directly instead of working with Eq. (3).<sup>[38,42]</sup> By renormalizing the NOs via their occupation numbers,  $|\tilde{\zeta}(t)\rangle = \sqrt{\eta_j(t)} |\zeta(t)\rangle$ , Refs. [42–44] showed that the equations of motion for the orbitals and those for the occupation numbers can be instead combined

into one for each renormalized-orbital, which is numerically far more stable than the coupled equations for  $\eta_i(t)$  and  $|\xi_i(t)\rangle$ . By studying model two-electron systems, for which the exact 2RDM is known in terms of the NOs and occupation numbers,<sup>[45]</sup> Refs. [42–44] could propagate the renormalized NOs in strong fields, with the only approximation being propagating a finite number of orbitals. Even relatively few orbitals gave very good results for challenging phenomena in correlated strong-field dynamics: autoionization, Rabi oscillations, and non-sequential double-ionization. For more than two electrons, one will however run again into the challenge of finding an accurate approximation for the 2RDM in terms of the renormalized NOs.

The progress and applications in time-propagating RDMs as described above has been relatively recent (the use of RDMs in static electronic structure theory is much older and more established), although the BBGKY equations were written down sixty years ago. This is partly because of the instabilities stemming from violating  $N$ -representability when one truncates the hierarchy, or the inability of the adiabatic approximations for the functionals  $\rho_2[\rho_1]$  to change occupation numbers, as reviewed above. TDDFT, on the other hand, formulated about thirty years ago,<sup>[3,27]</sup> has seen significant applications, especially for the calculations of excitations and response, while the past decade has witnessed exciting explorations into strong-field regime. As discussed above, the Runge–Gross states that all observables can be obtained from the one-body density, but, instead of working directly with the density, TDDFT operates by propagating a system of non-interacting electrons, the Kohn–Sham system, that reproduces the exact interacting density. The potential in the equation for the Kohn–Sham orbitals is defined such that  $N$  non-interacting electrons evolving in it have the same time-dependent one-body density as the true interacting problem. One component of this potential is the exchange–correlation potential, a functional of the density  $\rho$ , the initial interacting state  $\Psi$ , and the initial choice of Kohn–Sham orbitals  $\Phi$  in which to begin the propagation,  $v_{XC}[\rho; \Psi_0, \Phi_0](\mathbf{r}, t)$ . In almost all of the real-time non-perturbative calculations, an adiabatic approximation is used, in which the time-evolving density is inserted in a ground-state functional approximation, neglecting the dependence on the initial-states and the history of the density. This has produced usefully accurate results in a range of situations, e.g. modeling charge-transfer dynamics in photovoltaic candidates,<sup>[46]</sup> ultrafast demagnetization in solids,<sup>[47]</sup> dynamics of molecules in strong fields.<sup>[48]</sup> Yet, there are errors, sometimes quite large,<sup>[49–53]</sup> and investigation of the behavior of the *exact* exchange–correlation potential reveals non-adiabatic features that are missing in the approximations in use today.<sup>[54–56]</sup> Further, when one is interested in observables that are not directly related to the density, additional “observable-functionals” are needed to extract the information from the Kohn–Sham system: simply evaluating the usual operators on the Kohn–Sham wavefunction is not correct, even when the exact exchange–correlation potential functional is used.<sup>[57–60]</sup> Although it is in principle possible to extract all observables from the Kohn–Sham system, it is not known how. A final challenge is that Kohn–Sham evolution maintains constant occupation numbers,

even with the exact functional, which results in strong exchange–correlation effects. The one-body nature of the Kohn–Sham potential means that the Kohn–Sham state remains a SSD throughout the evolution, even though the interacting system that it is modeling can dramatically change occupation numbers,<sup>[38,61]</sup> evolving far from an SSD (e.g., if a singlet single excitation gets appreciably populated during the dynamics). This leads to large features in the exact exchange–correlation potential that are difficult to model accurately.

So, although computationally attractive, one could argue that operating via a non-interacting reference leads to a more difficult task for functionals. This has motivated the revisiting of the 1RDM dynamics in recent years as discussed above: any one-body observable can be directly obtained from the 1RDM using the usual operators, and one does not need the effective potential to “translate” from a non-interacting system to an interacting system. This suggests the terms in the equation that contain the many-body physics could be easier to model. As discussed in the previous paragraphs, the difficulty then is to come up with approximations for the 2RDM that can change occupation numbers and maintain  $N$ -representability of the 1RDM. In this work, we implement the idea first introduced in Ref. [11], using a semiclassical approximation for the correlation term in Eq. (3).

#### Semiclassical-correlation driven TDHF

From now on we deal only with singlet states and consider only the spin-summed RDMs. We begin by extracting the correlation component of Eq. (3), by decomposing  $\rho_2$  via an SSD-contribution from Eq. (6), plus a correlation correction:

$$\rho_2(\mathbf{r}', \mathbf{r}_2, \mathbf{r}, \mathbf{r}_2, t) = \rho_2^{\text{SSD}}(\mathbf{r}', \mathbf{r}_2, \mathbf{r}, \mathbf{r}_2, t) + \rho_{2C}(\mathbf{r}', \mathbf{r}_2, \mathbf{r}, \mathbf{r}_2, t) \quad (9)$$

Then the last term of Eq. (3) can be written

$$\int d^3 r_2 f_{ee}(\mathbf{r}, \mathbf{r}', \mathbf{r}_2) \rho_2(\mathbf{r}', \mathbf{r}_2, \mathbf{r}, \mathbf{r}_2, t) = (v_H(\mathbf{r}, t) - v_H(\mathbf{r}', t)) \rho_1(\mathbf{r}', \mathbf{r}, t) + F_X(\mathbf{r}', \mathbf{r}, t) + v_{2C}(\mathbf{r}', \mathbf{r}, t) \quad (10)$$

where

$$v_H(\mathbf{r}, t) = \int d^3 r' \frac{\rho(\mathbf{r}', t)}{|\mathbf{r} - \mathbf{r}'|} \quad (11)$$

is the familiar Hartree potential of DFT and

$$F_X(\mathbf{r}', \mathbf{r}, t) = -\frac{1}{2} \int d^3 r_2 f_{ee}(\mathbf{r}, \mathbf{r}', \mathbf{r}_2) \rho_1(\mathbf{r}', \mathbf{r}_2, t) \rho_1(\mathbf{r}_2, \mathbf{r}, t) \quad (12)$$

is the Fock exchange matrix. The final term of Eq. (10) we refer to as the correlation potential:

$$v_{2C}(\mathbf{r}', \mathbf{r}, t) = \int d^3 r_2 f_{ee}(\mathbf{r}, \mathbf{r}', \mathbf{r}_2) \rho_{2C}(\mathbf{r}', \mathbf{r}_2, \mathbf{r}, \mathbf{r}_2, t) \quad (13)$$

Without  $v_{2C}$ , the propagation of Eq. (3) using the first two terms of Eq. (10), reduces to TDHF. In the present work, we

will evaluate  $v_{2C}$  via semiclassical Frozen Gaussian dynamics, so turn now to a short review of this.

### Frozen Gaussian dynamics

Semiclassical methods aim to approximate the solution of Eq. (1) via an expansion in  $\hbar$ ; the zeroth order recovers the classical limit while the first-order  $O(\hbar)$  terms are referred to as the semiclassical limit. For propagation, a popular example is the Heller–Herman–Kluk–Kay (HHKK) propagator<sup>[5–10,62–64]</sup> where the  $N$ -particle wavefunction at time  $t$  as a function of the  $3N$  coordinates, denoted  $\underline{\mathbf{r}} = \{\mathbf{r}_1, \dots, \mathbf{r}_N\}$ , is:

$$\Psi^{\text{FG}}(\underline{\mathbf{r}}, t) = \int \frac{d\mathbf{q}_0 d\mathbf{p}_0}{(2\pi\hbar)^N} \langle \underline{\mathbf{r}} | \mathbf{q}_t, \mathbf{p}_t \rangle C_{\mathbf{q}, \mathbf{p}, t} e^{iS_t/\hbar} \langle \mathbf{q}_0, \mathbf{p}_0 | \Psi_0 \rangle \quad (14)$$

where  $\{\mathbf{q}_t, \mathbf{p}_t\}$  are classical phase-space trajectories at time  $t$  in  $6N$ -dimensional phase-space, starting from initial points  $\{\mathbf{q}_0, \mathbf{p}_0\}$ . In Eq. (14),  $\langle \underline{\mathbf{r}} | \mathbf{q}, \mathbf{p} \rangle$  denotes the coherent state:

$$\langle \underline{\mathbf{r}} | \mathbf{q}, \mathbf{p} \rangle = \prod_{j=1}^{3N} \left( \frac{\gamma_j}{\pi} \right)^{1/4} e^{-\frac{\gamma_j}{2} (r_j - q_j)^2 + i p_j (r_j - q_j) / \hbar} \quad (15)$$

where  $\gamma_j$  is a chosen width parameter.  $S_t$  is the classical action along the trajectory  $\{\mathbf{q}_t, \mathbf{p}_t\}$ . Finally, each trajectory in the integrand is weighted by a complex pre-factor based on the monodromy (stability) matrix,  $C_{\mathbf{q}, \mathbf{p}, t}$  which guarantees the solution is exact to first order in  $\hbar$ . Computing this pre-factor is the most time-consuming element in the integral, scaling cubically with the number of degrees of freedom.

When the prefactor in Eq. (14) is set to unity, HHKK reduces to the simpler Frozen Gaussian (FG) propagation,<sup>[7]</sup> which is more efficient. As a consequence, it is no longer exact to order  $\hbar$  and the results are no longer independent of the choice of width parameter  $\gamma_j$ , unlike in HHKK. For our calculations we take  $\gamma_j = 1$ . Neither the HHKK propagation nor FG is unitary; typically we find the norm of the FG wavefunction decreases with time, and so we must renormalize at every time-step. In previous work,<sup>[12]</sup> the FG dynamics of electrons was investigated and found to give reasonable results for a number of different quantities and systems. Some of these will be referred to in the Results presented here.

### TDDMFG

In this work, we will implement the idea of Ref. [11] whereby a FG propagation, running parallel to a propagation of the 1RDM, is used to construct  $v_{2C}$ , which is then used in Eq. (10) and Eq. (3) to propagate the 1RDM. From the FG wavefunction given by Eq. (14), the 1RDM and 2RDM are computed and then used to construct:

$$v_{2C}^{\text{FG}}(\mathbf{r}', \mathbf{r}, t) = \int d^3 r_2 f_{ee}(\mathbf{r}, \mathbf{r}', \mathbf{r}_2) \rho_{2C}^{\text{FG}}(\mathbf{r}', \mathbf{r}_2, \mathbf{r}, \mathbf{r}_2, t) \quad (16)$$

where  $\rho_{2C}^{\text{FG}}$  is found by inverting Eq. (9):

$$\rho_{2C}^{\text{FG}}(\mathbf{r}', \mathbf{r}_2, \mathbf{r}, \mathbf{r}_2, t) = \rho_2^{\text{FG}}(\mathbf{r}', \mathbf{r}_2, \mathbf{r}, \mathbf{r}_2, t) - \rho^{\text{FG}}(\mathbf{r}_2, t) \rho_1^{\text{FG}}(\mathbf{r}', \mathbf{r}, t) + \frac{1}{2} \rho_1^{\text{FG}}(\mathbf{r}', \mathbf{r}_2, t) \rho_1^{\text{FG}}(\mathbf{r}_2, \mathbf{r}, t) \quad (17)$$

We then insert this into Eq. (16), and propagate Eq. (3) with the last term evaluated using Eq. (16). We refer to this coupled dynamics as TDDMFG, meaning time-dependent density-matrix propagation with Frozen-Gaussian correlation.

The scheme of Ref. [11] takes advantage of the “forward-backward” nature of the propagation of the 2RDM (i.e., there is both a  $\Psi(t)$  and a  $\Psi^*(t)$ ), which leads to some cancellation of the oscillatory phase for more than two electrons. We also observe that the spatial permutation symmetry of the initial-state is preserved during the evolution (since the Hamiltonian is for identical particles, exchanging coordinate-momentum pairs of two electrons does not change the action). We will study here two-electron singlet states where the wavefunction is spatially symmetric under exchange of particles. In the FG propagation, although the energy of each classical trajectory is conserved in the absence of external fields, the energy of the FG wavefunction constructed from these trajectories is not guaranteed to be. As noted earlier, the norm is not conserved either and the wavefunction must be renormalized at each time. Thus, in general it is unlikely that energy will be conserved in the TDDMFG scheme.

### Computational details

The phase-space integral in Eq. (14) is performed using Monte Carlo integration, with the distribution of  $M$  initial phase-space points weighted according to a simple Gaussian initial distribution. In principle this method scales as  $\sqrt{M}$ , however the oscillatory phase from the action  $S_t$  can make the FG propagation difficult to converge and thus a large number of trajectories are often needed. This, in turn, means that parallelization of the numerical computation of Eq. (14) is needed. Fortunately, the main task is “embarrassingly parallel” as each classical trajectory can be calculated separately, however construction in real space of the FG wavefunction, 2RDM, 1RDM, and Eq. (16) is time-consuming and also required parallelization (in a manner similar to the Fock exchange matrix calculations discussed below). To avoid performing these costly procedures at every time step, we used a linear-interpolation of Eq. (16) which only required its construction every  $D_V$  timesteps. We tested that the results were converged with respect to  $D_V$ , finding accurate results for values as high as  $D_V = 200$  for a timestep of  $dt = 0.001$  au for the cases we studied.

The 1RDM propagation was performed via the predictor-corrector method combined with an Euler forward-stepping algorithm. All quantities were calculated on a real-space grid and the derivatives in Eq. (3) were done using a 3-point finite difference rule.

Calculation of the Fock exchange matrix, Eq. (12), also required parallelization, as it has the worst scaling (cubic) with respect to the number of grid points of the remaining quantities. Parallelization often contains additional subtleties which can make the problem non-trivial, thus in order to parallelize

efficiently, the problem was first transformed to resemble a more typical problem in parallel computing. To detail this procedure, it is convenient to switch to a matrix representation:

$$\rho := \rho_{nm} = \rho_1(\mathbf{r}_n, \mathbf{r}_m) \quad (18)$$

where  $\mathbf{r}_n$  is the  $n$ th point of the real-space grid. We then define a new matrix

$$\tilde{\rho} := \tilde{\rho}_{nm} = A_{nm} \rho_{nm} \quad (19)$$

where

$$\mathbf{A} := A_{nm} = V_{\text{INT}}(\mathbf{r}_n, \mathbf{r}_m) \quad (20)$$

which is then used to construct

$$\mathbf{C} = \rho \tilde{\rho} := C_{nm} = \sum_k \rho_{nk} \tilde{\rho}_{km} \quad (21)$$

The Fock exchange matrix can then be written as

$$\mathbf{F}_x = \frac{\Delta x}{2} (\mathbf{C}^\dagger - \mathbf{C}) \quad (22)$$

in the case when the Fock integral is evaluated via quadrature and  $\Delta x$  is the grid spacing. Thus, we have reduced the calculation of the Fock exchange integral to the calculation of  $\mathbf{C}$ , which only involves a matrix–matrix multiplication. In parallel computing, matrix–matrix multiplication is a well-studied problem for which standard solutions exist and thus could be easily implemented in our code without additional difficulty.

## RESULTS

In this section, we present the results of the TDDMFG formulation for various time-dependent problems and compare the results to the TDHF (i.e.,  $v_{2C}=0$ ), the pure FG, and the exact cases. In order to compare with the exact results, we work in 1D and focus on two-electron systems, as it allows us to solve the full TDSE in a reasonable time with reasonable computational resources.

We first tested our TDDMFG propagation algorithm by coupling to the exact dynamics, i.e. we used the exact wavefunction to calculate the exact  $v_{2C}$  at each time which is then used within the 1RDM propagation to verify it recovers the exact dynamics. To remove any error due to the initial ground state we start the FG dynamics in the exact GS wavefunction and the 1RDM propagation in the exact GS density matrix.

Each of TDHF and FG calculations on their own can yield reasonably good results for particular cases, thus the goal of the coupled TDDMFG propagation should be to either improve upon both, or at least, improve the results in scenarios where one or the other performs poorly.

### Hooke's atom

We begin by studying Hooke's atom in 1D, which consists of a harmonic external potential:

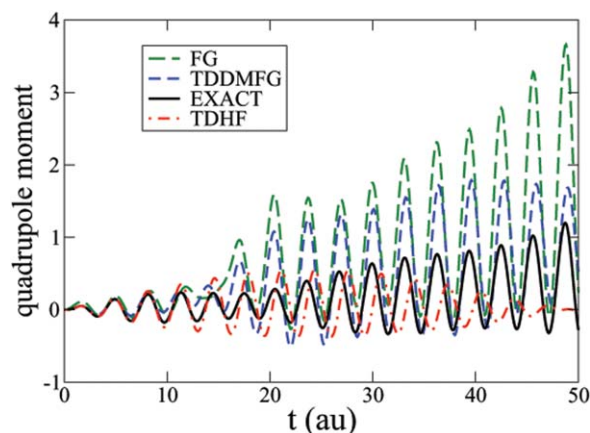


Figure 1. Comparison of the quadrupole moment for Hooke's atom driven by a quadratic field at frequency  $\omega = 2$  for the exact case, TDHF, FG, and the coupled TDDMFG. For the FG run, a total of 100,224 classical trajectories were used.

$$v_{\text{ext}}(x) = \frac{1}{2} k_0 x^2 \quad (23)$$

and a softened Coulomb interaction between the electrons:

$$V_{\text{INT}}(x', x) = \frac{1}{\sqrt{(x-x')^2 + 1.0}} \quad (24)$$

In our first application we drive the system by applying an oscillating quadrupole field

$$\delta v_{\text{ext}}(x, t) = k(t) x^2 \quad (25)$$

where  $k(t) = -0.025 \sin(2t)$  and  $k_0 = 1$ . The frequency of this perturbation is chosen to be resonant with an allowed excitation of the system. We then compare in Figure 1 the change in the quadrupole moment relative to the ground state quadrupole ( $Q_0$ ),

$$Q(t) = \int dx \rho(x) x^2 - Q_0 \quad (26)$$

as computed via exact propagation, TDHF, FG semiclassical dynamics, and TDDMFG propagation. In this case we see an improvement to both the TDHF and the FG calculations. While the exact quadrupole is seen to continue increasing in amplitude over time, the TDHF does not, and in fact oscillates in a beating pattern. This is partly due to the fact that TDHF spectra cannot describe this particular excitation (which will be discussed in more detail later) and leads to an off-resonance Rabi oscillation. However even running TDHF at the resonance frequency of TDHF does not show Rabi oscillations either; although the quadrupole begins to grow, it ultimately fails because of the spurious detuning effect explained in Ref. [65]. The FG, in contrast, overestimates the amplitude of the oscillations, while the TDDMFG coupled dynamics lies in between these two extremes and is much closer to the exact result. In previous work we found that the quadrupole is more sensitive than other quantities to the number of trajectories used in our

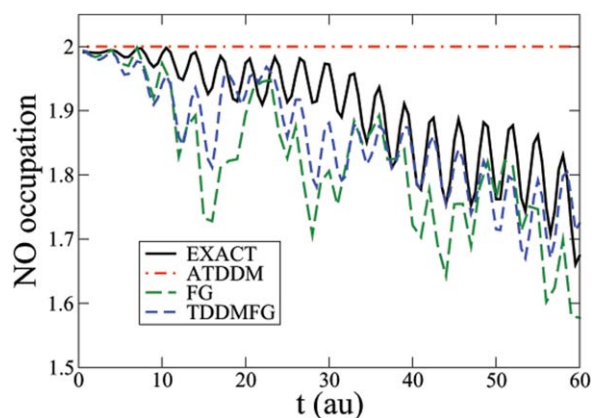


**Figure 2.** Evolution of the occupation of the highest occupied natural orbital for the driven Hooke's atom in the exact case, TDHF, FG, and TDDMFG.

FG calculation, in this case 100,224. Thus we could expect better agreement if we further increase the number of trajectories. It is interesting to note that all three approximate calculations work reasonably well for the first 10 au.

Buoyed on by this success, we next examine the NO occupation numbers to probe the 1RDM in more detail than the quadrupole, an averaged expectation value, can provide. As noted in the earlier review, a major shortcoming of adiabatic functionals in TDDMFT is their inability to change these occupations. As can be seen in Figure 2 this behavior manifests itself as straight lines, labeled ATDDM, constant at the initial state NO occupations. This is also true for the TDHF case shown previously. Since we spin-sum, the NOs go between 0 and 2, and we plot the highest occupied NO occupation, which this case begins very close to 2, indicating the initial state is strongly of an SSD character. The time-dependence of this occupation is shown in Figure 2. The exact value decreases toward a value of 1 as the system becomes excited and the wavefunction moves away from SSD-like state. In Ref. [12], it was shown that FG propagation can quite accurately capture the evolution of the NO occupations, so the question is whether the coupled dynamics of TDDMFG is also able to do so. Examining the TDDMFG values, we see that TDHF coupled to the FG correlation is able to evolve the occupations accurately. In fact TDDMFG is slightly better than the pure FG values where FG has sometimes spuriously large oscillations.

Although the amplitude of the oscillations of the TDDMFG quadrupole is closer to those of the exact than the FG oscillations, the phase of the oscillations of the latter is closer to the exact case than the TDDMFG case. This becomes more evident carrying the propagation out to longer times. This can be understood from considering the resonant frequencies of the system: the frequency of the perturbation  $k(t)$  is on-resonance with an excitation of the exact system which FG in fact correctly describes. The TDDMFG excitation frequency is however shifted slightly leading to the difference in phase observed here. We will now examine the respective excitation frequencies of each method in more detail.

Turning to how well the TDDMFG captures excitation spectra, we focus in particular on so-called double excitations (defined loosely as excitations which have a large fraction of a doubly excited state character, with respect to the SSD ground state of a non-interacting reference system<sup>[66]</sup>). It is known that these excitations are missing from all TDDFT spectra calculations within the adiabatic approximation. Since TDHF is equivalent to adiabatic exact exchange in TDDFT for the 2-electron case studied here, we do not see double excitations in the uncoupled 1RDM TDHF spectra. This point is illustrated in the upper panel of Figure 3 which shows the TDHF power spectra. The spectra are calculated via the linear response method, utilizing a "kicked" initial state defined as:

$$\Psi_0(x, y) = e^{ik(x^n + y^n)} \Psi_{GS}(x, y) \quad (27)$$

where  $\Psi_{GS}$  is the ground-state wavefunction,  $k$  is a small constant, and  $n$  is an integer (we define a quadratic kick as  $n = 2$  and a cubic kick as  $n = 3$ ). An expression for the initial 1RDM can be easily derived from this. A dipole kick ( $n = 1$ ) is commonly used when calculating optical spectra as it corresponds to an electric field consisting of a  $\delta$ -function at time  $t = 0$

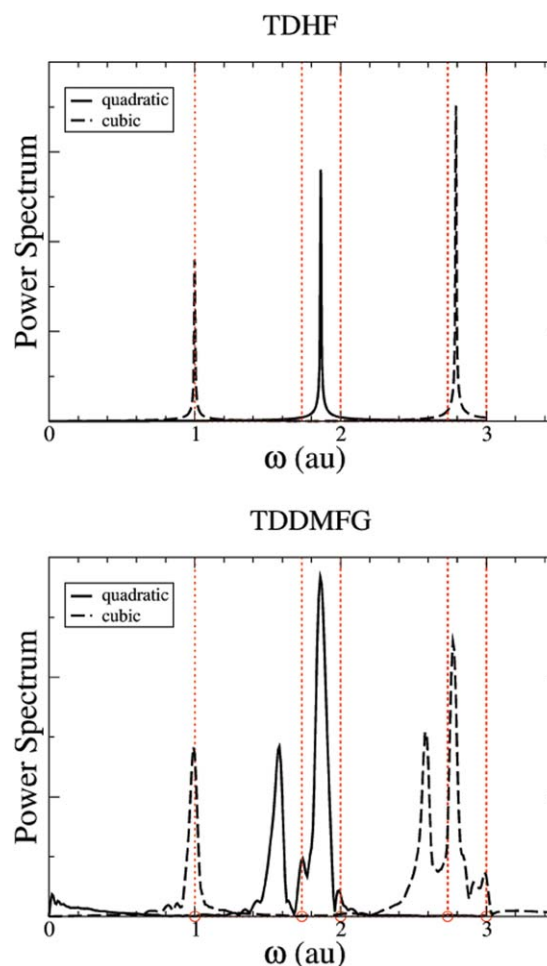


**Figure 3.** Excitation spectra of Hooke's atom calculated via linear response with quadratic/cubic kicked initial states and the Fourier transform of the relevant moment for TDHF (upper panel) and TDDMFG (lower panel).

**Table 1.** The singlet excitation frequencies  $\omega_n = E_n - E_0$ , where the ground-state energy is  $E_0 = 1.774040$  a.u., solved exactly for Hooke's atom, and the corresponding TDHF, FG, and TDDMFG values as calculated by real-time linear response.

Exact	TDHF	FG	TDDMFG
1.000000	0.99	1.0	0.99
1.734522	1.86	1.6	1.58
2.000000	–	2.0	1.86
2.734522	2.79	2.6	2.58
3.000000	–	3.0	2.77

which excites all dipole allowed excitations.<sup>[67]</sup> However due to symmetries of Hooke's atom, to access the double excitations, higher moment kicks were necessary.<sup>[12]</sup> To obtain the spectra, for each run we calculate the appropriate moment (e.g., quadrupole moment for quadratic kicks) and Fourier transform to frequency space to reveal the excitation peaks.<sup>[12]</sup> In the TDHF case, we do not see the pair of excitations peaks at frequencies (1.73,2.0), nor the pair (2.73,3.0) but instead see a single peak in between. This behavior is commonly seen for TDDFT calculations with an adiabatic approximation, where a frequency-dependent XC kernel is required to split the peak

into two separate excitations<sup>[66,68]</sup>; any adiabatic approximation in TDDMFT will also only display one peak.<sup>[35]</sup>

Moving to the lower panel of Figure 3, we plot the TDDMFG spectra calculated in the same manner. It can be seen that including  $v_{2C}^{FG}$  into the TDHF propagation correctly splits the single peak into two peaks, for both the quadratic and cubic kick cases. Thus we have demonstrated that our coupled dynamics does indeed capture double excitations. Identifying the position of the peaks, we compare in Table 1 the values given by each method for the lowest 5 excitations of Hooke's atom. It was found in Ref. [12] that FG on its own also describes double excitations quite well, and in fact is exact for certain excitations in Hooke's atom. This is due to the fact that the Hamiltonian becomes separable in center-of-mass and relative coordinates, and that in the center-of-mass coordinate is a simple harmonic oscillator.<sup>[12]</sup> It is well-known that harmonic potentials are a special case for semiclassical methods as they often perform exactly. With this in mind, although the value of the TDDMFG frequencies are worse than the pure FG values, they are competing with a special case, but in fact the splitting between the peaks is better described by the TDDMFG. In particular, in the second multiplet, the exact splitting is 0.27, while that of the TDDMFG is 0.28, improved over the bare FG result of 0.4 (and obviously over TDHF

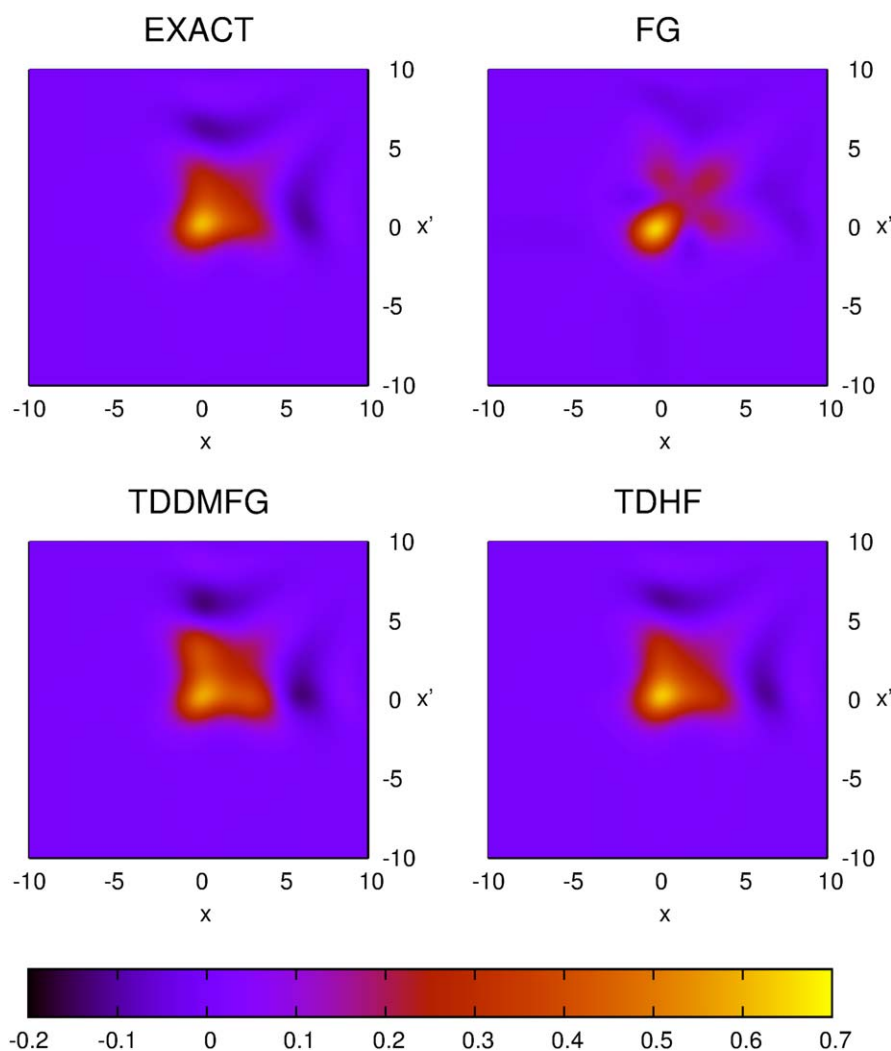


**Figure 4.** Comparison of the real part of the density matrix at time  $T = 10$  au for strongly driven soft-Coulomb Helium.



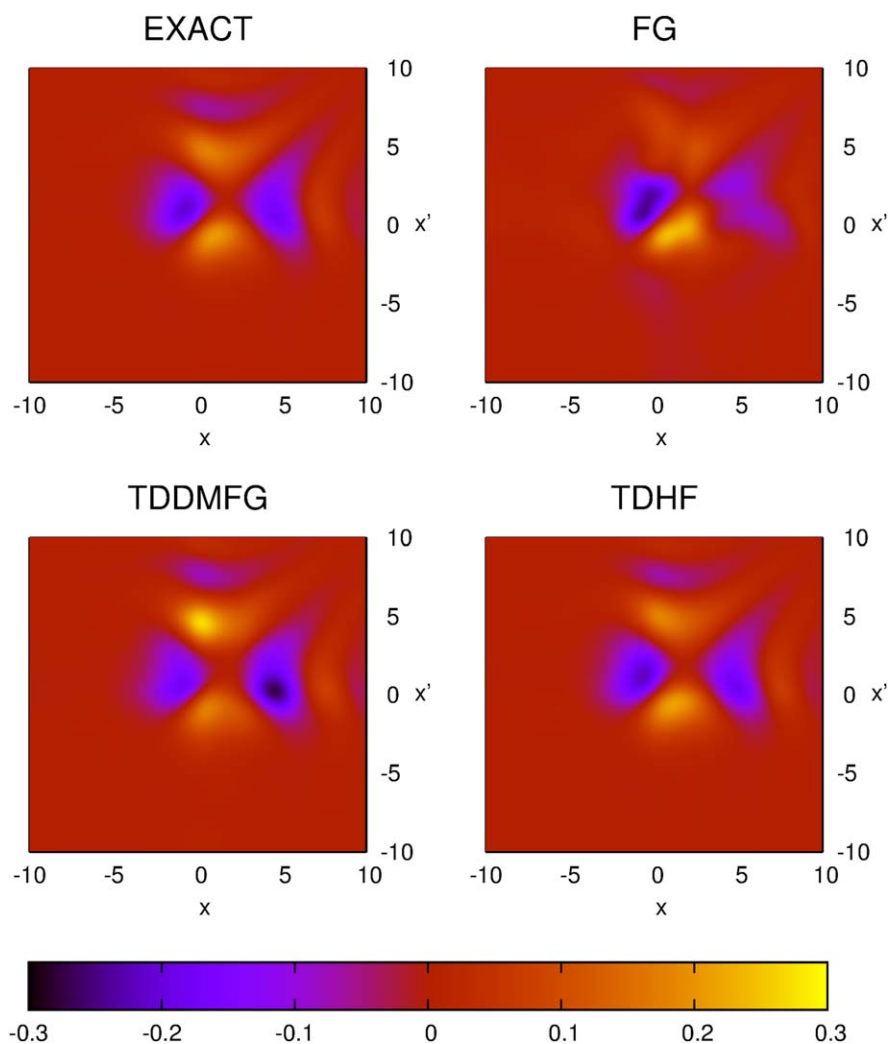


Figure 5. Comparison of the imaginary part of the density matrix at time  $T = 10$  au for strongly driven soft-Coulomb Helium.

where there is no peak). We emphasize again that these excitations are completely missing in the TDHF case, or in any adiabatic TDDFT or TDDMFT functional. It is better to have the excitations shifted slightly from the exact result than to not describe them at all.

### Soft-Coulomb Helium

We now move to the more realistic case of soft-Coulomb Helium where the external potential is:

$$v_{\text{ext}}(x) = -\frac{2}{\sqrt{x^2+1.0}} \quad (28)$$

which mimics the 3D case as for large  $x$  it decays as  $-1/|x|$ . In the previous case of Hooke's atom, we saw that the problem was well described by the FG dynamics whereas the TDHF performed poorly (i.e., not changing the NO occupations or capturing double excitations). Driving the TDHF with FG correlation in TDDMFG interestingly improved over FG for the NO occupations and quadrupole moment, with slightly worse performance for the double-excitations. For dynamics in the soft-Coulomb Helium case we will see, in contrast, that the FG is worse than the TDHF

for some quantities. Will the coupled dynamics of TDDMFG improve the situation? As detailed in Ref. [12], this case is much more difficult for the FG method due to classically auto-ionizing trajectories (where one electron gains energy from the other and ionizes while the other slips below the zero-point-energy), thus a far greater number of trajectories are required. Ref. [12] discussed how in a truly converged Frozen Gaussian calculation, the contributions from these unphysical trajectories cancel each other out, but a very large number of trajectories are required; otherwise methods to cut out their contribution to the semiclassical integral can be used. In the presented calculations, 2,000,448 trajectories were used and all were kept.

We apply a strong laser pulse with a linearly-switched-on electric field:

$$\epsilon(t) = \frac{1}{\sqrt{2}} \cos(0.5t) \begin{cases} \frac{t}{20} & t \leq 20 \\ 1 & t > 20 \end{cases} \quad (29)$$

which is included in our Hamiltonian via the dipole approximation, i.e.  $\delta v_{\text{ext}}(x) = \epsilon(t)x$ . We begin by examining the 1RDM itself at time  $T = 10$  au: the real part is shown in Figure 4 and

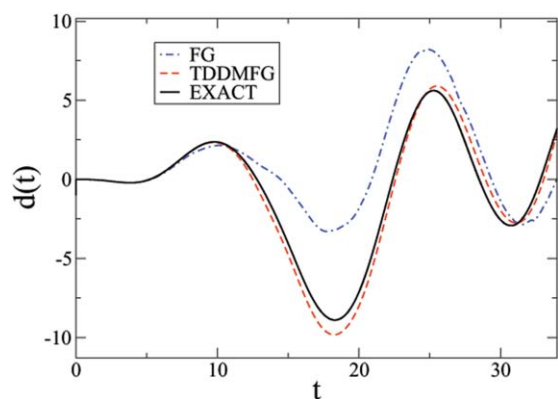


**Figure 6.** The dipole moment during the strongly driven soft-Coulomb Helium for the exact calculation, the FG, and the TDDMFG. The FG calculation required 2,000,448 classical trajectories. Note that the TDHF calculation (not shown) is very accurate during this time period.

the imaginary part in Figure 5. At this time, while the structure of the FG 1RDM is broadly correct, it can be seen that the TDHF 1RDM is much closer to the exact. The TDDMFG 1RDM also captures more of the correct structure compared to the pure FG case, although it generally overestimates the peaks and valleys. Thus, while the  $v_{2C}^{FG}$  is constructed from the poorer FG calculation, the TDDMFG follows more closely the more accurate TDHF description.

We next turn to the dipole moment which is plotted in Figure 6. The TDHF (not shown) essentially matches the exact case, whereas the FG performs quite poorly, particularly during the second optical cycle. The TDDMFG, in contrast, is performing particularly well and follows very closely the exact result, even at times greater than  $T = 10$  au, likely due to the guidance of the TDHF component in the evolution.

At this point one might conclude that the TDDMFG is behaving correctly, however the good results for the 1RDM and dipole moment are masking the fact that the underlying description suffers from a major error, described below.

As was the case for Hooke's atom, a more thorough examination of the method is given by studying the NO occupa-

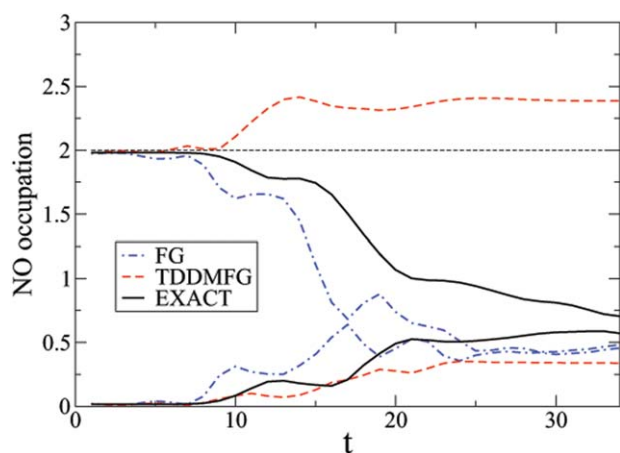


**Figure 7.** The evolution of the two-highest occupied natural orbital occupations for the strongly driven soft-Coulomb Helium. We omit the ATDDM occupations as they stay constant at their initial values.

tions. The highest two NO occupations are plotted in Figure 7 where the strong field causes a large change in their values. In fact we see that the FG description of the NO occupations is working better than we previously anticipated, albeit overestimating their change. Again the TDHF occupations (not shown) are constant, fixed at their initial values. At  $T = 10$  au, the exact 1RDM is still dominated by the highest occupied natural orbital, explaining why the TDHF appeared so good at this time.

Unfortunately in the TDDMFG case, we see that the highest occupation rises above 2 thus violating the exact condition for  $N$ -representability of the 1RDM (positive semidefiniteness). The effect of this is quite drastic as the density develops negative regions, due to having negative occupations (the sum of the occupations remains 2, thus an increase above 2 is accompanied by negative values). At  $T = 10$  au the value of the highest NO is only slightly above 2 and so this bad behavior has yet to truly manifest itself. The FG NO occupation at  $T = 10$  au is underestimated, consistent with the FG 1RDM being not so accurate. At later times, none of the methods provide a particularly good description of the 1RDM structure, with the TDHF remaining the closest, despite its constant occupation number, but the TDHF momentum densities are not good. The TDDMFG 1RDM resembles the TDHF but with exaggerated highs and lows, and unphysical negative regions, manifest also in the momentum density.

It is a frustrating situation where neither the FG nor TDHF on their own violates the  $N$ -representability condition, and FG does evolve the occupation numbers unlike any adiabatic approximation, however coupling FG correlation to TDHF in the TDDMFG leads violation of  $N$ -representability. We speculate this is due to a mismatch in correlation potential and the Hartree-exchange terms as there is no mechanism to provide feedback between the two calculations. Implementing a dynamical purification scheme along the lines of that in Ref. [18] that iteratively decreases the magnitude of the negative occupation numbers should be investigated.

## Conclusions

The TDDMFG dynamics which uses a Frozen Gaussian calculation to construct an approximation to the correlation potential in 1RDM propagation gives mixed results. On one hand, it was shown for Hooke's atom to be a significant improvement over all adiabatic 1RDM functionals as it can vary the natural orbital occupations reasonably accurately. Furthermore it was shown that double excitations, which are difficult to capture with the commonly-used TDDFT method and adiabatic TDDMFT, can be accurately described with the TDDMFG formalism. On the other hand, for soft-Coulomb Helium the method was seen to fail drastically giving the unphysical result of negative density due to violation of an exact constraint. Further work is required to understand why this violation occurs and then hopefully to then use this information to prevent it from occurring. This same problem, violation of the positive semi-definiteness, was also found in other recent approaches propagating RDMs with approximate correlation terms.<sup>[17,18]</sup> Dynamical purification

schemes along the line of that successfully used in Ref. [18] could be very helpful here. Indeed understanding how the FG correlation potential changes NO occupation or includes double excitations could be used to construct better approximations for TDDMFT. Finally, in this work, we studied systems of only two electrons, whereas we might expect that (semi)classical methods work best for large numbers of particles, and it remains to be seen whether the problems we encountered become less significant for larger systems.

An advantage of using a semiclassical scheme to evaluate the correlation term is that initial state dependence is automatically taken care of: in general reconstructions, whether one begins in an excited state or ground-state, the same approximation for the 2RDM in terms of the 1RDM is assumed. This is known to be incorrect; several different initial wavefunctions and different initial 2RDM's can give rise to the same initial 1RDM.<sup>[69,70]</sup> The resulting correlation effect is clearly different depending on the wavefunction, but this effect is ignored in all reconstructions in use today. For this reason, it seems worthwhile to pursue further investigations of a semiclassical-correlation driven TDHF, once the *N*-representability problem is taken care of, especially since in many simulations of non-equilibrium dynamics of interest today, the problem starts in a photo-excited state.

## Acknowledgments

Authors thank Robert Numrich and Richard Walsh, of the CUNY HPC center, for useful discussions concerning the parallelization of our code. We also thank Ali Akbari and Javad Hashemi for very useful comments on the manuscript. PE acknowledges support by SFB 762 of the Deutsche Forschungsgemeinschaft. NM thanks NSF (Grant CHE-1162784) for financial support. The CUNY HPCC is operated by the College of Staten Island and funded, in part, by grants from the City of New York, State of New York, CUNY Research Foundation, and National Science Foundation Grants CNS-0958379, CNS-0855217 and ACI 1126113.

**Keywords:** double excitations · Frozen Gaussian · time dependent density matrix functional theory · reduced density matrix · semiclassical methods

How to cite this article: P. Elliott, N. T. Maitra. *Int. J. Quantum Chem.* **2016**, *116*, 772–783. DOI: 10.1002/qua.25087

- [1] D. A. Mazziotti, Ed. *Advances in Chemical Physics*, Vol. 134: Reduced-Density-Matrix Mechanics: With Application to Many-Electron Atoms and Molecules; Wiley: Hoboken NJ, **2007**.
- [2] P. Elliott, F. Furche, K. Burke, In *Reviews in Computational Chemistry*; K. B. Lipkowitz, T. R. Cundari, Eds.; Wiley: Hoboken, NJ, **2009**; p. 91.
- [3] M. A. L. Marques, N. T. Maitra, F. Nogueira, A. Rubio, E.K.U. Gross, Eds. *Fundamentals of Time-Dependent Density Functional Theory*; Springer-Verlag: Berlin, **2012**.
- [4] K. Pernal, K. J. H. Giesbertz, In *Density Functional Methods for Excited States*, N. Ferre, M. Filatov, and M. Huix-Rotllant, Eds., Springer International Publishing Switzerland, Vol. 368 of *Topics in Current Chemistry*, **2015**, 125–184.
- [5] J. H. van Vleck, *Proc. Natl. Acad. Sci. USA* **1928**, *14*, 178.
- [6] L. S. Schulman, *Techniques and Applications of Path Integration*; Wiley, USA, **1981**.
- [7] E. J. Heller, *J. Chem. Phys.* **1981**, *75*, 2923.
- [8] W. H. Miller, *Faraday Disc. Chem. Soc.* **1998**, *110*, 1.
- [9] M. Thoss, H. Wang, *Ann. Rev. Phys. Chem.* **2004**, *55*, 299.
- [10] K. G. Kay, *Annu. Rev. Phys. Chem.* **2005**, *56*, 255.
- [11] A. K. Rajam, I. Raczowska, N. T. Maitra, *Phys. Rev. Lett.* **2010**, *105*, 113002.
- [12] P. Elliott, N. T. Maitra, *J. Chem. Phys.* **2011**, *135*, 104110.
- [13] (a) N. N. Bogoliubov, *J. Phys. USSR* **1946**, *10*, 265; (b) N. N. Bogoliubov, K. P. Gurov, *J. Exp. Theor. Phys.* **1947**, *17*, 614; (c) J. Yvon, *Actual. Sci. Ind.* **1935**, *203* (Paris, Hermann); (d) J. G. Kirkwood, *J. Chem. Phys.* **1946**, *14*, 180; (e) *ibid* **1947**, *15*, 72; (f) M. Born, H. S. Green, *Proc. Roy. Soc. A* **1946**, *188*, 10.
- [14] M. Bonitz, *Quantum Kinetic Theory*; B. G. Teubner: Stuttgart Leipzig, **1998**.
- [15] S. J. Wang, W. Cassing, *Ann. Phys. NY* **1985**, *159*, 328.
- [16] F. Colmenero, C. Pérez del Valle, C. Valdemoro, *Phys. Rev. A* **1993**, *47*, 971.
- [17] A. Akbari, M. J. Hashemi, A. Rubio, R. M. Nieminen, R. van Leeuwen, *Phys. Rev. B* **2012**, *85*, 235121.
- [18] F. Lackner, I. Brezinová, T. Sato, K. L. Ishikawa, J. Burgdörfer, *Phys. Rev. A*, **2015**, *91*, 023412.
- [19] D. A. Mazziotti, *Chem. Phys. Lett.* **1998**, *289*, 419.
- [20] A. J. Coleman, *Rev. Mod. Phys.* **1963**, *35*, 668.
- [21] D. A. Mazziotti, *Phys. Rev. Lett.* **2012**, *108*, 263002.
- [22] D. A. Mazziotti, *Phys. Rev. E* **2002**, *65*, 026704.
- [23] D. R. Alcoba, F. J. Casquero, L. M. Tel, E. Prez-Romero, C. Valdemoro, *Int. J. Quantum Chem.* **2005**, *102*, 620.
- [24] D. B. Jeffcoat, A. E. DePrince, *J. Chem. Phys.* **2014**, *141*, 214104.
- [25] R. Requist, *Phys. Rev. A* **2012**, *86*, 022117.
- [26] K. Pernal, O. Gritsenko, E. J. Baerends, *Phys. Rev. A* **2007**, *75*, 012506.
- [27] E. Runge, E. K. U. Gross, *Phys. Rev. Lett.* **1984**, *52*, 997.
- [28] K. Giesbertz, *J. Chem. Phys. Phys.* **2015**, *143*, 1.
- [29] A. M. K. Müller, *Phys. Lett. A* **1984**, *105*, 446.
- [30] S. Goedecker, C. J. Umrigar, *Phys. Rev. Lett.* **1998**, *81*, 866.
- [31] M. Buijss, E. J. Baerends, *Mol. Phys.* **2002**, *100*, 401.
- [32] O. V. Gritsenko, K. Pernal, E. J. Baerends, *J. Chem. Phys.* **2005**, *122*, 204102.
- [33] P. Levina, M. Piris, *J. Chem. Phys.* **2005**, *123*, 214102.
- [34] S. Sharma, J. K. Dewhurst, N. N. Lathiotakis, E. K. U. Gross, *Phys. Rev. B* **2008**, *78*, 201103.
- [35] K. Giesbertz, E. J. Baerends, O. Gritsenko, *Phys. Rev. Lett.* **2008**, *101*, 033004.
- [36] R. Requist, O. Pankratov, *Phys. Rev. A* **2010**, *81*, 042519.
- [37] R. Requist, O. Pankratov, *Phys. Rev. A* **2011**, *83*, 052510.
- [38] H. Appel, E. K. U. Gross, *Europhys. Lett.* **2010**, *92*, 23001.
- [39] K. J. H. Giesbertz, O. V. Gritsenko, E. J. Baerends, *Phys. Rev. Lett.* **2010**, *105*, 013002.
- [40] K. J. H. Giesbertz, O. V. Gritsenko, E. J. Baerends, *J. Chem. Phys.* **2012**, *136*, 094104.
- [41] R. van Meer, O. V. Gritsenko, K. J. H. Giesbertz, E. J. Baerends, *J. Chem. Phys.* **2013**, *138*, 094114.
- [42] M. Brics, D. Bauer, *Phys. Rev. A* **2013**, *88*, 052514.
- [43] J. Rapp, M. Brics, D. Bauer, *Phys. Rev. A* **2014**, *90*, 012518.
- [44] M. Brics, J. Rapp, D. Bauer, *Phys. Rev. A* **2014**, *90*, 053418.
- [45] P. O. Löwdin, H. Shull, *Phys. Rev.* **1956**, *101*, 1730.
- [46] C. A. Rozzi, S. M. Falke, N. Spallanzani, A. Rubio, E. Molinari, D. Brida, M. Maiuri, G. Cerullo, H. Schramm, J. Christoffers, C. Lienau, *Nat. Commun.* **2013**, *4*, 1602.
- [47] K. Krieger, J. K. Dewhurst, P. Elliott, S. Sharma, E. K. U. Gross, *J. Chem. Theory Comput.* **2015**, *11*, 4870.
- [48] I. Bocharova, I. Bocharova, R. Karimi, E. F. Penka, J-P. Brichta, P. Lassonde, X. Fu, J-C. Kieffer, A. D. Bandrauk, I. Litvinyuk, J. Sanderson, and F. Légaré, *Phys. Rev. Lett.* **2011**, *107*, 063201.
- [49] M. Ruggenthaler, D. Bauer, *Phys. Rev. Lett.* **2009**, *102*, 233001.
- [50] S. Raghunathan, M. Nest, *J. Chem. Theory Comput.* **2011**, *7*, 2492.
- [51] R. Ramakrishnan, M. Nest, *Phys. Rev. A* **2012**, *85*, 054501.
- [52] S. Raghunathan, M. Nest, *J. Chem. Theory Comput.* **2012**, *8*, 806.
- [53] B. F. Habenicht, N. P. Tani, M. R. Provorse, C. M. Isborn, *J. Chem. Phys.* **2014**, *141*, 184112.
- [54] P. Elliott, J. I. Fuks, A. Rubio, N. T. Maitra, *Phys. Rev. Lett.* **2012**, *109*, 266404.
- [55] J. I. Fuks, P. Elliott, A. Rubio, N. T. Maitra, *J. Phys. Chem. Lett.* **2013**, *4*, 735.
- [56] J. D. Ramsden, R. W. Godby, *Phys. Rev. Lett.* **2012**, *109*, 036402.

- [57] F. Wilken, D. Bauer, *Phys. Rev. Lett.* **2006**, *97*, 203001.  
 [58] F. Wilken, D. Bauer, *Phys. Rev. A* **2009**, *76*, 023409.  
 [59] A. K. Rajam, P. Hessler, C. Gaun, N. T. Maitra, *J. Mol. Struct. Theochem.* **2009**, *914*, 30.  
 [60] N. Henkel, M. Keim, H. J. Lüdde, T. Kirchner, *Phys. Rev. A* **2009**, *80*, 032704.  
 [61] K. Luo, J. I. Fuks, E. Sandoval, P. Elliott, N. T. Maitra, *J. Chem. Phys.* **2014**, *140*, 18A515.  
 [62] M. F. Herman, E. A. Kluk, *Chem. Phys.* **1984**, *91*, 27.  
 [63] E. Kluk, M. F. Herman, H. L. Davis, *J. Chem. Phys.* **1986**, *84*, 326.  
 [64] F. Grossmann, A. L. Xavier, *Phys. Lett. A* **1998**, *243*, 243.  
 [65] J. I. Fuks, K. Luo, E. D. Sandoval, N. T. Maitra, *Phys. Rev. Lett.* **2015**, *114*, 183002.  
 [66] P. Elliott, S. Goldson, C. Canahui, N. T. Maitra, *Chem. Phys.* **2011**, *391*, 110.  
 [67] K. Yabana, T. Nakatsukasa, J. I. Iwata, G. F. Bertsch, *Phys. Stat. Sol. (B)* **2006**, *243*, 1121.  
 [68] N. T. Maitra, F. Zhang, R. J. Cave, K. Burke, *J. Chem. Phys.* **2004**, *120*, 5932.  
 [69] P. Elliott, N. T. Maitra, *Phys. Rev. A* **2012**, *85*, 052510.  
 [70] (a) N.T. Maitra, K. Burke, *Phys. Rev. A* **2001**, *63*, 042501; (b) N.T. Maitra, K. Burke, *Phys. Rev. A* **2001**, *64*, 039901 (Erratum).

---

Received: 5 November 2015  
 Revised: 16 December 2015  
 Accepted: 4 January 2016  
 Published online 1 February 2016